

Torque Multiplication and Stable Range Tradeoff in Parallel Plate Angular Electrostatic Actuators With Fixed DC Bias

Ajay Pareek, *Member, IEEE*, Mehmet R. Dokmeci, *Member, IEEE*, Shivalik Bakshi, and Carlos H. Mastrangelo, *Member, IEEE*

Abstract—The nonlinear torque-voltage characteristics in two-terminal electrostatic actuators can be utilized to magnify the torque generated by a drive voltage applied to one electrode if a fixed dc bias is applied to the other. The resulting torque is enhanced by torque gain factor $G_\tau > 1$, and the drive voltage is effectively multiplied by voltage gain factor $G_V > 1$ compared to that of an actuator with no dc bias. These gain factors are generated at the expense of a reduced stable range. In this paper, we study and determine experimentally the tradeoff between torque and voltage gains versus stable range for one-dimensional (1-D), three-terminal, parallel-plate angular electrostatic actuators under dc bias. Simple approximate analytical relations are derived for voltage and torque gain as functions of applied dc bias voltage. We demonstrate that for voltage gains of 2–4, the angular range is marginally reduced. [1361]

Index Terms—Electrostatic actuators, micromirror, parallel-plate, torque magnification.

I. INTRODUCTION

ANGULAR parallel-plate electrostatic actuators such as those shown in Fig. 1 have received much attention recently as candidate devices for implementing optical fiber switches [1]–[4]. In these applications large mirror sizes (~ 1 mm) and tilt angles $\theta \geq 5^\circ$ are generally required to establish low loss connections. These specifications inevitably lead to high voltage (>100 V) drives because the steering planar electrodes have to be placed at a relatively large vertical gap from the mirror. It is therefore highly desirable to find techniques that reduce the drive voltage to levels compatible with conventional low-voltage electronics. Among several possible voltage reduction techniques (mechanical advantage [5], raised electrodes [6], nonlinear springs [7], etc) the torque gain technique is relatively easy to implement, and it does not rely on complicated fabrication steps or a major redesign of the actuator.

Manuscript received June 17, 2004; revised May 10, 2005. Subject Editor N. C. Tien.

A. Pareek is currently a consultant in the private sector (e-mail: apareek@ieee.org).

M. R. Dokmeci is with the Department of Electrical and Computer Engineering, Northeastern University, Boston, MA 02115 USA.

S. Bakshi is with BioScale, Inc., Cambridge, MA 02139 USA (e-mail: shivalik@hotmail.com).

C. H. Mastrangelo is with the Department of Electrical and Computer Engineering, Case Western Reserve University, Cleveland, OH 44106-7071 USA (e-mail: carlos.mastrangelo@case.edu).

Digital Object Identifier 10.1109/JMEMS.2005.859072

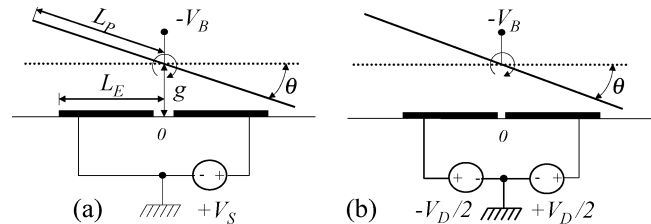


Fig. 1. Schematic cross section of typical angular electrostatic actuator showing different bias configurations. (a) The device can be driven single ended or (b) differentially. The significant parameter is the voltage swing at the drive electrodes.

The torque gain technique uses a fixed dc bias V_B and the nonlinear dependence of torque with voltage to reduce the drive requirement [9], [10] (see Fig. 1). For example, in the single ended drive of Fig. 1(a), the torque voltage relationship at low deflection angles is approximately of the form

$$\begin{aligned} \tau &\approx K \cdot (V_B + V_S)^2 - K \cdot (V_B)^2 \\ &= K \cdot \left(2 \cdot \left(\frac{V_B}{V_S} \right) + 1 \right) \cdot V_S^2 \\ &= K \cdot G_\tau \cdot V_S^2 \\ &= K \cdot (G_V \cdot V_S)^2 \end{aligned} \quad (1)$$

where K is

$$K = \frac{1}{2} \left(\frac{dC}{d\theta} \right)_{\theta=0} \quad (2)$$

Equation (1) shows that if $V_B > 0$ the torque is magnified by gain $G_\tau > 1$, and the effect of the drive voltage is magnified by voltage gain $G_V > 1$. If $V_B > V_S$ large torque (and voltage) gains are achievable; however as V_B is increased, the actuator becomes unstable and pulls-in; therefore this method has been largely used for digital or bistable applications, such as the Texas Instruments digital micromirror device [10].

In this paper, we investigate the suitability of this technique for analog drive applications. We first calculate the relationship between gain and stable range of operation as functions of dc bias and actuator dimensions, and these relationships are observed experimentally on a silicon micromachined mirror structure. The relationship equations yield a general design methodology for maximization of stable range at a given dc bias.

The straightforward use of a dc biasing scheme for torque magnification comes at a cost. If the electrostatic torque $\tau_e(\theta)$ is a monotonically increasing nonlinear function of displacement

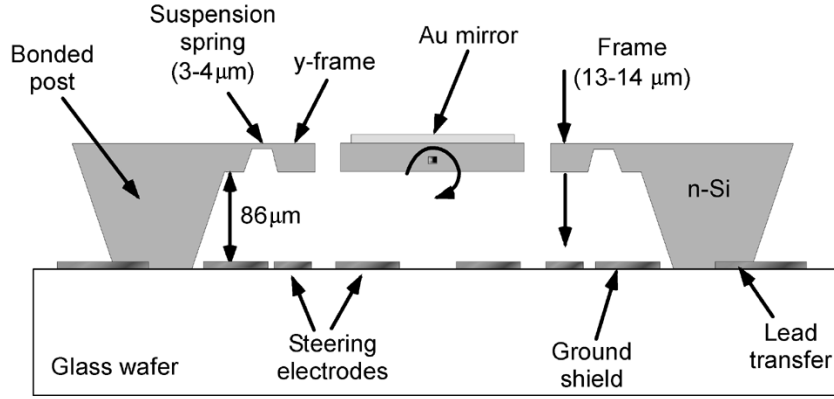


Fig. 2. Cross section of bulk micromachined mirror used for measurements. The entire structure is made of single crystal silicon.

angle, the nonlinearity produces a spring softening effect which is magnified by the presence of the bias. The effective spring constant for the device with bias becomes

$$k_{\text{eff}} = k_{\text{spring}} - \left(\frac{d\tau_e}{d\theta} \right) = k_{\text{spring}} - \left(\frac{d^2C}{d\theta^2} \right) \cdot V_B^2 < k_{\text{spring}} \quad (3)$$

hence the bias decreases the resonant frequency of the structure resulting in extended settling times. The closer the device is to instability, the longer the settling time is under conventional linear control schemes. The extended settling time however can be largely eliminated if the device is driven differentially with a digital-pulsed control method [11].

II. DEVICE STRUCTURE

Torque and voltage gain measurements were carried out on bulk micromachined angular mirror actuator made of silicon-on-insulator (SOI). Fig. 2 shows the cross-section of the device [8]. The device is fabricated by anodically bonding a 7740 Pyrex glass wafer with patterned metal electrodes to an SOI wafer with 100- μm -thick device layer. Prior to bonding, the silicon device layer is anisotropically etched to precisely define the thickness of both flexures and mirror support plate. Electrical lead transfers are made by overlapping the glass metal onto the silicon, and lead wires are routed to bonding pads located at the edge of the chip. After bonding, the silicon carrier substrate is dissolved in TMAH and the buried oxide is removed. Next, the gold mirrors are defined, and the gimbal structure is patterned using deep RIE. Fig. 3 shows a SEM photograph of the completed device array. Even though this device permits rotation on two axes, the angular measurements were carried out on the frame actuator axis which conforms to the diagram of Fig. 1. More details about the device construction and performance are presented in [8].

III. SIMPLIFIED DEFLECTION MODEL

We consider the structure shown in Fig. 1(a) with fixed negative bias voltage $-|V_B|$ applied to the movable plate and single ended drive voltage V_S applied to one of the drive electrodes. The actuator has electrode of width w and a torsional spring of constant k . For this simplified model the flexures are assumed to be infinitely stiff vertically.

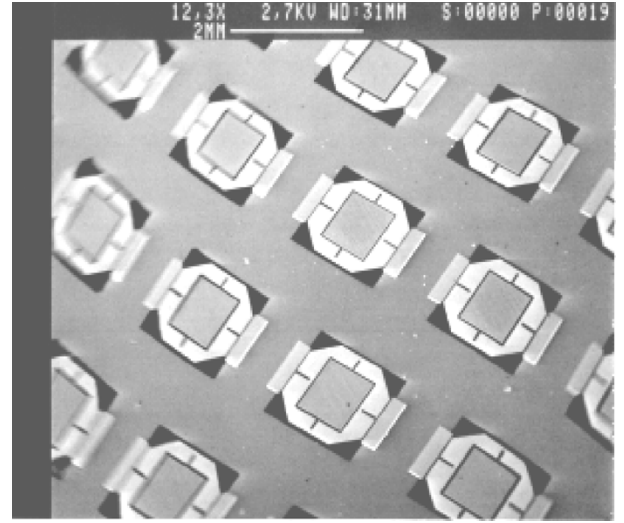


Fig. 3. SEM photograph of a MEMS mirror array.

The equilibrium angle of the actuator can be determined from the minimum of the system energy U_T versus angular deflection θ . This energy is the sum of the mechanical energy stored in the spring and the electrical energy of the charge stored in the two drive electrodes and the power supplies. Using the coenergy formulation [12]

$$U_T = \frac{1}{2}k \cdot \theta^2 - \frac{V_B^2}{2}C_L(\theta) - \frac{(V_B + V_S)^2}{2}C_R(\theta) \quad (4)$$

where $C_L(\theta)$ and $C_R(\theta)$ are the capacitances of the left and right electrodes to the tiltable plate. Assuming low deflection angles, $\tan(\theta) \approx \theta$, and ignoring fringing field contributions, these capacitances can be calculated analytically yielding

$$U_T \approx \left(\frac{kg^2}{2L_E^2} \right) \left[n^2 - \frac{M}{n} \log\left(\frac{1+n}{1-n} \right) - \frac{b(b+2)M}{n} \log\left(\frac{1}{1-n} \right) \right] \quad (5)$$

where $n = (L_E\theta/g)$ is the normalized actuator deflection, $b = (V_S/V_B)$, $M = (\epsilon_o V_B^2 w L_E^3 / k g^3)$, and \log is the natural log function. L_E is length of the electrode, and g is the vertical gap between mirror rotation axis and the glass substrate. Equation (5) is valid if L_E/g and w/g are large and fringing fields are negligible. If these ratios are not large the capacitances must be increased by an appropriate geometric correction factor.

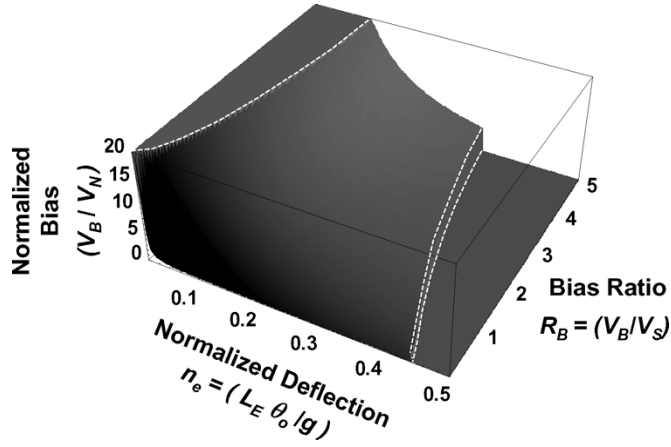


Fig. 4. Relation between normalized bias, deflection angle and bias gain. A plot of $(\partial^2 U_T / \partial n^2)$ reveals that the truncated surface is stable.

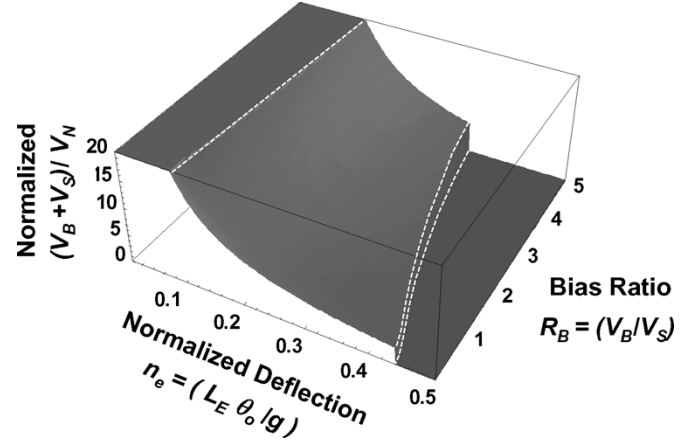


Fig. 5. Normalized voltage sum as a function of deflection and bias ratio.

If $b = 0$, corresponding to zero drive voltage, it is well known [9] that the energy curve has one stable minima at $\theta = 0$ between two unstable maxima equidistant from the origin. The angle difference between the two maxima defines the stable range. The energy curve has three distinct equilibria as long as the dc bias is sufficiently low such that parameter $M < 3/2$. At high dc biases when $M \geq 3/2$ the three equilibria merge to produce a single maximum, and the actuator becomes unstable. Clearly, this instability threshold limits the maximum bias voltage that can be applied when $V_S = 0$ for a given L_E/g .

In practice, if $V_S > 0$ the stable range is reduced even more further limiting the achievable gains. The equilibrium deflection, n_e for a given M and b can be determined by setting $(dU_T/dn) = 0$ in (5) at $n = n_e$ (the equilibrium value) and solving for M as shown in (6) at the bottom of the page. In general, it is desirable to minimize the drive voltage (and b) for a fixed maximum required rotation angle θ_o and maximum available bias V_B . The worst case stable drive condition develops when V_S is equal to the voltage required for a maximum rotation angle θ_o ; hence we set the normalized deflection to its maximum value $n_e = (L_E \theta_o / g)$ obtaining the expression (7) at the bottom of the page where the normalizing voltage V_N

$$V_N = \sqrt{\frac{k\theta_o^3}{\epsilon_o w}} \quad (8)$$

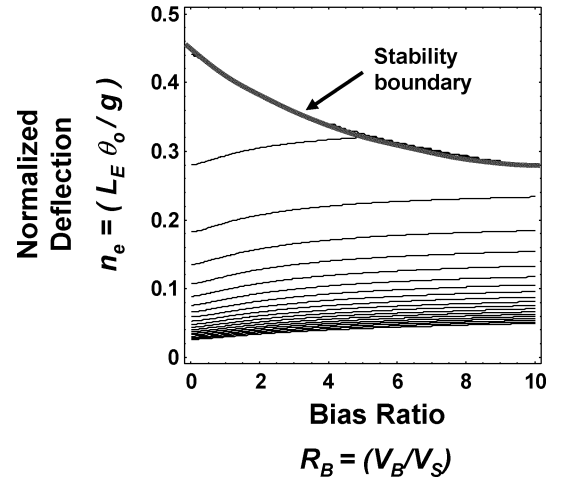


Fig. 6. Contours of normalized voltage sum as a function of deflection and bias ratio. At high ratios the contours are nearly independent of bias ratio.

is only a function of the spring constant k , electrode width w and maximum rotation angle θ_o . For convenience we also define the bias ratio parameter $R_B = b^{-1}$. Using these definitions we can now plot the relationship between V_B , n_e and R_B as shown in Fig. 4. Any value of V_B above this surface causes pull-in, and for any value below it, the device is stable. The truncation of the surface along the normalized deflection axis corresponds to the pull-in instability boundary as the smooth surface yields

$$M = \frac{2n_e^3(1-n_e^2)}{n_e(2+b(2+b)(1+n_e)) - (1-n_e^2) \left[\log\left(\frac{1+n_e}{1-n_e}\right) + b(2+b) \log\left(\frac{1}{1-n_e}\right) \right]} \quad (6)$$

$$\frac{V_B}{V_N} = \left(\frac{2(1-n_e^2)}{n_e(2+b(2+b)(1+n_e)) - (1-n_e^2) \left[\log\left(\frac{1+n_e}{1-n_e}\right) + b(2+b) \log\left(\frac{1}{1-n_e}\right) \right]} \right)^{\frac{1}{2}} \quad (7)$$

unstable equilibria for larger n_e (because $(\partial^2 U_T / \partial n^2)|_{n_e} \leq 0$). Note that for large $R_B > 1$ and small $n_e < 0.25$ the surface becomes nearly independent of bias ratio R_B , and in principle, large biases can be applied at the expense of reduced stable n_e . This is more noticeable if we plot the normalized quantity $(V_B + V_S)/V_N$ as shown in Fig. 5. For larger n_e the surface is weakly dependent of the bias ratio as shown in the contour plot of Fig. 6 showing nearly parallel contours for $R_B > 2$.

The thick line in Fig. 6 indicates the stability boundary. Note that for zero dc bias, the device is stable for $n_e < 0.45$ (ignoring fringe fields). The stability boundary in Fig. 6 suggests that for most practical bias ratios the maximum stable $n_e \approx 0.25$.

For $n_e \approx 0.25$ and using (7), the function

$$\frac{(V_B + V_S)}{V_N} = \frac{V_B}{V_N} \cdot (1 + b) = f(n_e, b) \approx 9.5 - 3\sqrt{\frac{b}{b+1}} \quad (9)$$

has a range $6.5 \leq f(n_e, b) \leq 9.5$. A useful first order approximation is thus obtained if the nonlinear function of b is replaced by its average

$$(V_B + V_S) \approx f(n_e) \cdot V_N = V_A \approx 7 \cdot \sqrt{\frac{k\theta_o^3}{\varepsilon_o w}}. \quad (10)$$

Equation (10) tells us that to first order if L_E , g , and θ_o are fixed, at high bias ratios and maximum deflection *the sum of the bias and drive voltage is approximately constant*. Therefore the maximum bias that can be applied while keeping the device stable is $V_B = V_A$, and this voltage is also the drive voltage required for maximum angle deflection when $V_B = 0$. The effect of the dc bias voltage is hence expressed in terms of a voltage gain. From these observations, at maximum deflection, the last term in (1) indicates that $V_A = G_V \cdot V_S$. Using this result and (10) we obtain

$$G_V = \frac{V_A}{V_S} = \frac{V_A}{(V_A - V_B)} = \frac{1}{\left(1 - \frac{V_B}{V_A}\right)}. \quad (11)$$

Due to fringing effects and the variation of $f(n_e, b)$ with R_B , a more practical semi-empirical expression is

$$G_V \approx \frac{1}{\left(1 - \frac{aV_B}{V_{S_o}}\right)} \quad (12)$$

where V_{S_o} is the experimental voltage required to drive the full range with zero bias and a is a fitting factor, and the torque gain is

$$G_\tau = (G_V)^2 \approx \frac{1}{\left(1 - \frac{aV_B}{V_{S_o}}\right)^2} \quad (13)$$

which is simply the square of the voltage gain.

Even though the equations presented here are highly simplified, the experimental data presented below suggest that they are approximately valid. They also provide a systematic procedure for choosing the bias and device parameters for a given range. For example, (10) tells us that V_B should be set to the maximum voltage available but less than V_A . Once V_B is set, the voltage gain is calculated from (11). With G_V known one may select L_E/g so that n_e stays within the stability region of Fig. 6

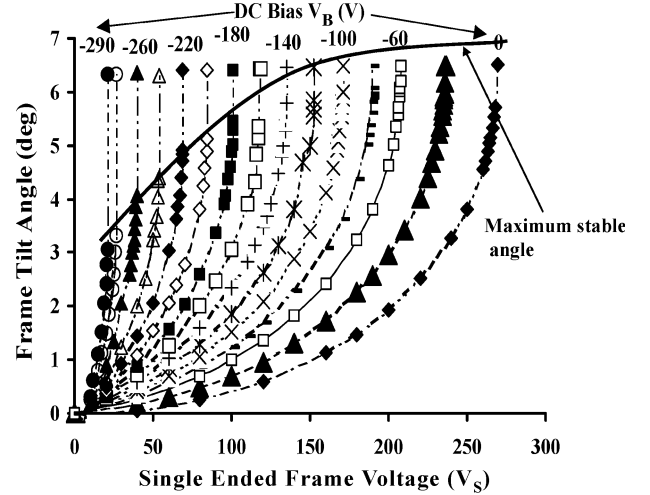


Fig. 7. Single-ended deflection of actuator for different dc biases.

(and near the assumed $n_e \approx 0.25$). Furthermore, if the device length (the extent of the movable plate from its axis of rotation) is known, the minimum gap g can be determined from the clearance requirements for maximum deflection θ_o . With known n_e and g , a unique value for L_E is obtained.

IV. EXPERIMENTS AND ANALYSIS OF DATA

The devices shown in Fig. 2 were subjected to various bias and single-ended drive conditions. The electrode length was $L_E = 195 \mu\text{m}$, width $w = 600 \mu\text{m}$ and the gap $g = 86 \mu\text{m}$. Each device had two sets of orthogonal torsional flexures with expected total $k \approx 1.3 \times 10^{-8} \text{ Nm/rad}$. Angular measurements were performed using a Zygo NewView 5032 interferometer with automated data acquisition system.

Fig. 7 shows deflection curves for outer frame as a function of single ended drive voltage V_S for different dc bias voltage V_B . The single ended drive voltage is reduced as the bias voltage is increased, and the stable angular range (at the onset of pull-in) is gradually reduced. For zero bias, the device pulls-in at about 6° . The maximum measured stable normalized deflection, $n_e = 0.24$ which should be stable (according to Fig. 6) when it is below 0.45. Therefore the device should not pull-in, but it does. The origin of this discrepancy is the fringing field effect which was ignored in the calculation. For this device, the ratios $L_E/g = 2.2$ and $w/g = 6.9$ are insufficiently large for fringing field effects to be neglected.

A simple correction factor at low-deflection angles can be added by effectively enlarging L_E and w [15]

$$(L_E)_{\text{eff}} \approx L_E + 0.77 \cdot g; \quad (w)_{\text{eff}} \approx w + 0.77 \cdot g \quad (14)$$

yielding $(n_e)_{\text{eff}} \approx 0.34$ which according to Fig. 6, becomes unstable at large bias gains causing the range reduction.

Using this approximation, a fit of the zero bias deflection curve yields $k \approx 1.9 \times 10^{-8} \text{ Nm/rad}$ in rough agreement with the expected value. From these we calculated $V_N \approx 46 \text{ V}$ and $V_A = 319 \text{ V}$. Fig. 8 shows the single ended voltage gain achieved as a function of the dc bias with fitted $V_A = 305 \text{ V}$.

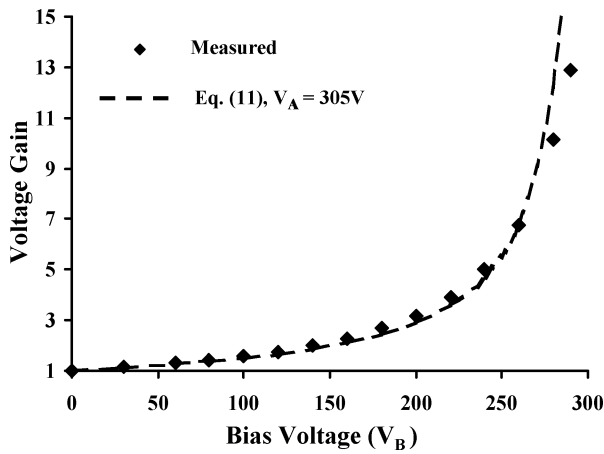


Fig. 8. Single-ended voltage gain for maximum angular range as a function of dc bias voltage.

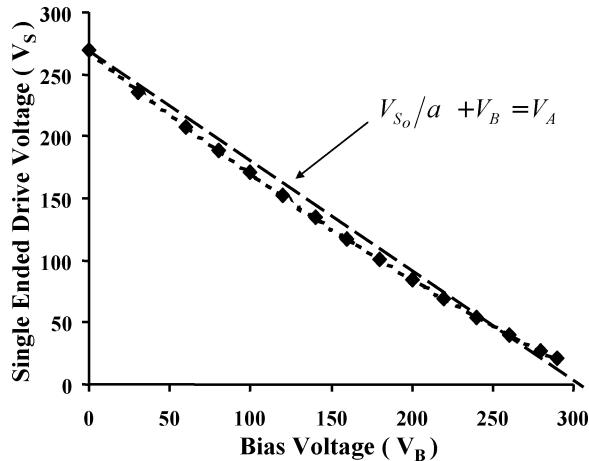


Fig. 9. Single-ended drive voltage required for maximum deflection for a given dc bias.

Note that the curve qualitatively resembles (12) and provides a good fit with experimental data with $a \approx 0.9$. The simplified equation overestimates the voltage gain at high biases due to the higher (than average) value of $f(n_e, b)$.

Fig. 9 shows the experimental single ended voltage for different biases at maximum stable deflection. The curve is almost a straight line as predicted by (10), but the slope suggests the form $V_{S_o}/a + V_B = V_A$.

Fig. 10 shows the measured stable deflection angle (half range) that can be achieved for different voltage gains. For gains of 2–4× the angular range is marginally reduced, but at a gain of 10, the angular range is reduced by half. The simplified model surface of Fig. 6 predicts a more modest range reduction of 30% when fringing field approximations of (14) are used.

V. SUMMARY

In this paper, we examined the relationship between the maximum stable deflection angle, the voltage gain, and the dc bias in an electrostatic angular actuator. A simplified model was constructed yielding a three dimensional surface that relates these three parameters in terms of the physical actuator dimensions. The model predicts that for maximum range, the

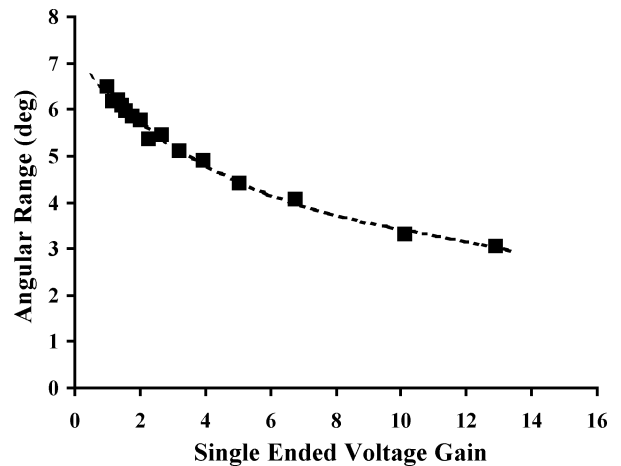


Fig. 10. Stable maximum deflection angle versus (stable) voltage gain. There is little loss in the angular range for gains 2–4×.

weighted sum of the bias and drive voltage is roughly constant, and the maximum bias that can be used is roughly equal to the full range single-ended drive voltage at zero bias. Furthermore, stable large voltage gains can be achieved making low voltage actuation of the drive electrodes possible.

The constant sum relation and the expression of the voltage gain versus bias are in reasonably good agreement with the experimental data. We also observed that as the voltage gain is increased, the maximum stable deflection angle is reduced. A practical voltage gain of 2–4× causes a marginal reduction of the stable range of deflection.

REFERENCES

- [1] S. H. Hinton, *An Introduction to Photonic Switching Fabrics*. New York: Kluwer Academic/Plenum, 1993.
- [2] D. Bishop, C. R. Giles, and G. P. Austin, "The Lucent LambdaRouter: MEMS technology of the future here today," *IEEE Commun. Mag.*, vol. 40, no. 3, pp. 75–79, Mar. 2002.
- [3] T. J. Brosnihan, S. A. Brown, A. Brogan, C. S. Gormley, D. J. Collins, S. J. Sherman, M. Lemkin, N. A. Polce, and M. S. Davis, "Optical IMEMS—a fabrication process for MEMS optical switches with integrated on-chip electronics," in *Proc. 12th International Conference on Solid State Sensors, Actuators, and Microsystems*, Boston, MA, Jun. 2003, pp. 1638–1642.
- [4] D. R. Peale, P. B. Chu, S. Park, N. H. Bonadeo, S. Lee, and M. Tsai, "Sidewall Electrodes for Electrostatic Actuation and Capacitive Sensing," U.S. Pat. 6 480 645, Nov. 2002.
- [5] J. H. Smith *et al.*, "1200 mirror array integrated with CMOS for photonic switching," in *Proc. Solid-State Sensor, Actuator and Microsystems Workshop*, 2002, pp. 378–379.
- [6] T. D. Kudrle *et al.*, "Pull-in suppression and torque magnification in parallel plate electrostatic actuators with side electrodes," in *Proc. Solid-State Sensor, Actuator and Microsystems Workshop*, 2003, pp. 360–363.
- [7] E. S. Hung and S. D. Senturia, "Extending the travel range of analog-tuned electrostatic actuators," *J. Microelectromech. Syst.*, vol. 8, pp. 497–505, 1999.
- [8] M. R. Dokmeci, S. Bakshi, A. Pareek, M. Waelti, C. D. Fung, and C. H. Mastrangelo, "Bulk micromachined electrostatic beam steering micromirror array," in *Proc. IEEE/LEOS International Conference on Optical MEMS*, Lugano, Switzerland, Aug. 2003, pp. 15–16.
- [9] L. Hornbeck *et al.*, "Spatial Light Modulator," U.S. Patent 5 061 049, Oct. 29, 1991.
- [10] L. J. Hornbeck, "Deformable-mirror spatial light modulators," in *Proc. Spatial Light Modulators and Applications III, SPIE*, vol. 1150, 1990, pp. 86–102.
- [11] N. Yazdi, H. Sane, and C. H. Mastrangelo, "Application of sliding mode control to electrostatically actuated two-axis gimbaled micromirrors," in *Proc. IEEE American Control Conference*, vol. 5, Jun. 2003, pp. 3726–3731.

- [12] S. D. Senturia, *Microsystem Design*. New York: Kluwer Academic, 2000.
- [13] K. Seo, Y. Cho, and S. Youn, "A bulk-micromachined silicon micromirror for tunable optical switch applications," in *Proc. IEEE Conf. on Emerging Technologies and Factory Automation*, vol. 2, Nov. 1996, pp. 404–407.
- [14] H. Toshiyoshi, W. Piyawattanametha, C.-T. Chan, and M. C. Wu, "Linearization of electrostatically actuated micromachined 2D optical scanner," *J. Microelectromech. Syst.*, vol. 10, no. 2, pp. 205–214, Jun. 2001.
- [15] N. Van de Meijs and J. T. Fokkema, "VLSI circuit reconstruction from mask topology," *Integration*, vol. 2, pp. 85–119, 1984.



Ajay Pareek (M'04) received the Ph.D. degree in physics from the University of Notre Dame, Notre Dame, IN, in 1996.

He joined Texas Instruments (TI), Richardson, TX, in 1996 as a Process Development Engineer working on Digital Micromirror Device (DMD) fabrication, yield, and design improvement. At TI, he was responsible for successful transfer of DMD fabrication from R&D environment to high-volume manufacturing in TI's CMOS fab. He also served as a Project Manager in Next Generation Lithography program at International Sematech, Austin, TX as an assignee from TI. He joined Corning-Intellisense, Wilmington, MA, in 2000 as the Manager of MEMS Test and Reliability Group, where he led the effort to develop state-of-the-art optical MEMS test equipment and established programs for high speed optical and electrical characterization as well as reliability testing of MOEMS based 3-D cross-connects, spatial light modulators, and wavelength selective switches. He has published numerous papers in peer-reviewed journals and international conference proceedings. His research interests are in novel fabrication techniques for micro- and nanomechanical devices, integration of MEMS and CMOS, microactuators, microfluidics, and biological and optical applications of microsystems.

international Sematech, Austin, TX as an assignee from TI. He joined Corning-Intellisense, Wilmington, MA, in 2000 as the Manager of MEMS Test and Reliability Group, where he led the effort to develop state-of-the-art optical MEMS test equipment and established programs for high speed optical and electrical characterization as well as reliability testing of MOEMS based 3-D cross-connects, spatial light modulators, and wavelength selective switches. He has published numerous papers in peer-reviewed journals and international conference proceedings. His research interests are in novel fabrication techniques for micro- and nanomechanical devices, integration of MEMS and CMOS, microactuators, microfluidics, and biological and optical applications of microsystems.



Mehmet R. Dokmeci (S'89–M'00) received the B.S. (with distinction) and the M.S. degrees from the University of Minnesota, Minneapolis, and the Ph.D. degree from the University of Michigan, Ann Arbor, all in electrical engineering. His dissertation was on hermetic encapsulation of implantable microsystems for chronic use in living systems.

Currently, he is with Northeastern University, Boston, MA, and was previously at the University of Michigan developing wafer-scale vacuum packages. He has also worked for Corning-Intellisense

Corporation, Wilmington, MA, developing MEMS-based products for the telecommunications and lifesciences industries. His research interests are concentrated in all areas of micromachining and its applications to biomedical and optical devices, hermetic and vacuum packaging, and implantable biosensors and he has 26 technical publications in these areas.

Dr. Dokmeci is a Member of HKN.



Shivalik Bakshi received the B.S. degree in mechanical engineering from Concordia University, Montreal, QC, Canada, in 1997, and the M.S. in applied science from Simon Fraser University, Burnaby, BC, Canada, in 2000. His graduate research focused on the development of MEMS devices for optical applications.

From 2000 to 2003, he worked at Corning Intellisense, where he was responsible for fabricating MEMS devices for telecom, biomedical and microsensor applications. Currently, he is with

BioScale Inc., Cambridge, MA, where he is engaged in the development of microsensors for biological detection.

Mr. Bakshi was awarded the Micralyne Design Award in 1999 for demonstrating novel and industrially relevant research in the area of MEMS.



Carlos H. Mastrangelo (S'84–M'90) was born in Buenos Aires, Argentina, in 1960. He received the B.S., M.S., and Ph.D. degrees in electrical engineering and computer science from the University of California, Berkeley, in 1985, 1988, and 1991, respectively. His graduate work concentrated on the applications of microbridges in microsensor technology.

From 1991 through 1992, he worked at the Scientific Research Laboratory, Ford Motor Company, Dearborn, MI, developing microsensors for automotive applications.

From 1993 to 2002, he was an Associate Professor of Electrical Engineering and Computer Science at the Center for Integrated Microsystems, University of Michigan, Ann Arbor. From 2000 to 2003, he was Vice President of Engineering at Corning-Intellisense, Wilmington, MA. Currently, he is a Professor of Electrical Engineering at Case Western Reserve University, Cleveland, OH. His research focuses on microelectromechanical system applications and technology, microfluidic systems, and integration, design, and modeling of MEMS fabrication processes. His group is credited for being the first group to detect DNA separations on a microfluidic chip integrated with an on-chip detector. He is also widely credited for developing the first model for stiction phenomena in MEMS.

Dr. Mastrangelo received the AT&T Fellowship Award in 1987. In 1991, he received the Sakrison Award for the best dissertation in the department. He received the 1991 Counsel of Graduate Schools/University Microfilms Distinguished Dissertation Award for the best technical dissertation in the United States and Canada. He also received a 1994 NSF Young Investigator Award. In 2000 his group received the best paper of the year award at the Transactions of Semiconductor Manufacturing for his work on synthesis of fabrication process flows for MEMS structures. He has served as an editor for *Sensors and Actuators*, and participated in technical and organizing committees of numerous SPIE and IEEE conferences in the MEMS area. He currently serves on the Editorial Board of the JOURNAL OF MICROELECTROMECHANICAL SYSTEMS.